

Supporting Information

Extremely Fast Charging Lithium-ion Battery using Bio-Based Polymer-Derived Heavily Nitrogen Doped Carbon

Kottisa Sumala Patnaik^a, Rajashekar Badam^a, Yueying Peng^a, Koichi Higashimine^b, Tatsuo Kaneko^a, and Noriyoshi Matsumi^{a,*}

1. Experimental section

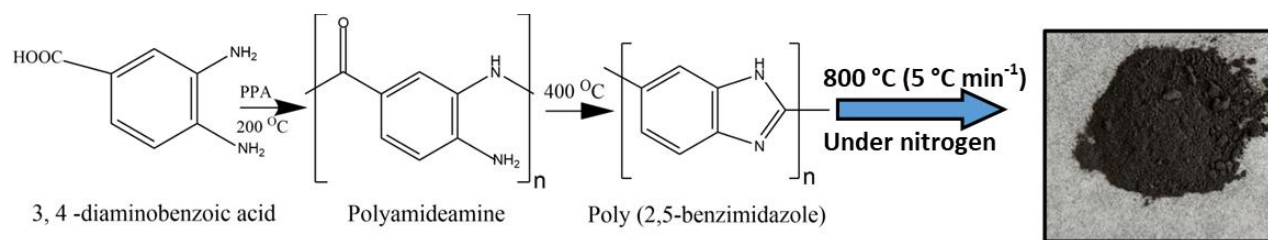
1.1 Materials

Bio-derived 3-amino-4-hydroxybenzoic acid (34AHBA) was given by Prof. C. Ogino (Kobe University) and 3,4-diaminobenzoic acid was converted from 34AHBA by the previously reported method¹⁴. Poly (phosphoric acid) (PPA) were purchased from Tokyo Chemical Industries (TCI, Tokyo, Japan). Potassium hydroxide (KOH) and hydrochloric acid were purchased from Kanto chemicals Co. Ltd. (Tokyo, Japan). 1.0 M LiPF₆ in EC: DEC= 50:50 (v/v), battery grade, was purchased from Sigma Aldrich. Acetylene black was purchased from Denka Japan Private Co. Ltd., polyvinylidene fluoride (PVDF) was purchased from Kureha Corporation, Japan (Mol. Wt. 2.8x10⁵ g mol⁻¹). N-Methyl 2-Pyrrolidone (NMP), 1st grade is purchased from FUJIFILM Wako Pure Chemical Corporation, Japan. Lithium metal was purchased from Honjo Metal Co., Ltd. containing thickness < 1mm. Copper foil (20 μm thick) was purchased from Nilaco corporation, Japan and commercial LiCoO₂ coated on aluminum foil was purchased from Piotrek, Japan with a capacity of 1.5 mAhcm⁻².

1.2 Synthesis of Polymer

Poly (2,5-benzimidazole) (AB-PBI) was synthesized with reference to the method earlier mentioned by Kaneko et.al. In brief, homo-polycondensation of 3,4-diaminobenzoic acid (3,4-DABA) (Scheme S1) was done by adding precursor (3, 4-DABA.2HCl) to the solvent (PPA) and heated at 200 °C for 14 h in nitrogen atmosphere. The obtained polymer was cooled to room temperature and was stirred in a beaker containing distilled water to wash off the unreacted precursors. After vacuum filtration, the polymer was dried at 180 °C overnight. The dried material was pulverized in a cryogenic crusher, JFC 300 at 1430 vibrations/min for 20 min to obtain a fine powder. The powdered polymer

was then dispersed in 10% KOH aq., solution and continuously stirred at room temperature overnight before filtering and washing with water until neutral pH. The resulted polymer powder was dried under vacuum at 80 °C for 8h.



Scheme 1: Synthesis of polymer and preparation method of carbon from polymer

1.3 Preparation of Carbon

The obtained polymer powder was pyrolyzed at 800 °C for 145 min at 5 °C per min rate of heating under nitrogen atmosphere. The obtained carbon was dispersed in 10 wt.% of 1M dil. HCl and vacuum filtered and washed with copious amount of water. The resulted carbon (PY-PBI-800) was dried at 80 °C under vacuum before further characterization.

2 Characterizations

Thermogravimetric Analysis was performed using Hitachi STA7200 thermal analysis system at a heating rate of 10 °Cmin⁻¹ and nitrogen flow of 200 mLmin⁻¹. FT-IR spectra was recorded using Perkin Elmer 100 FT-IR spectrometer. The spectra were averaged over 100 scans with a resolution of 2 cm⁻¹ in attenuated total reflection mode. The elemental composition and mapping of PY-PBI-800 was investigated using SEM-EDX on Hitachi TM3030 microscope connected to the EDS module. Transmission electron microscopy studies were carried out on scanning transmission electron microscope, JEM-ARM200F from JEOL Ltd at an acceleration voltage of 200 kV. X-ray photoelectron spectroscopy (XPS) was performed using Fisons instruments S-probe TM 2803 device. Powder X-ray diffraction (XRD) pattern of the sample was recorded using Smart Lab X-Ray Diffractometer, Rigaku with Cu K α radiation ($\lambda = 0.154$ nm, over the 2θ range of 10°–70° with a step size of 0.02°). Hitachi S-4500 field emission scanning electron microscopy (FE-SEM) instrument was used at 1.0 kV voltage. The elemental composition was evaluated (Table S1) by integrating the area under the curves for

respective XPS spectrum, followed by normalizing with respective sensitivity factors as shown in equation¹ (1).

$$\text{At. \%} = \frac{\frac{A_i}{SF_i}}{\sum_i \frac{A_i}{SF_i}} \times 100 \quad (1)$$

where i= Carbon/Nitrogen/Oxygen.

3 Electrochemical measurements

3.1 Electrode preparation: The slurry was prepared by ball milling PY-PBI-800 or graphite (active material), PVDF (binder), and Acetylene Black in the weight ratios 80:10:10 in NMP. Electrodes were coated by casting the as prepared slurry on the copper foil and using doctor blade with a coating thickness of 100 μm . The electrodes were dried for 16 hours at 80 $^{\circ}\text{C}$ in vacuum and were roll pressed at 80 $^{\circ}\text{C}$ maintaining a gap of 60 μm between the rollers. Further, the electrode discs (15 mm diameter) were punched for testing in coin cells. The mass loading of the electrodes was maintained at 0.85 mgcm^{-2} for anodic half cells. For the full cell studies the mass loading of Py-PBI-800 was maintained at around 5.7 mgcm^{-2} for balancing the capacity with the commercial cathode.

3.2 Battery fabrication: The electrochemical performance of the sample was evaluated using anodic half and full cells in CR-2025 type coin cells. Half-cells were fabricated using lithium as counter/reference electrode, 1.0 M LiPF_6 in 1:1 EC: DEC as electrolyte, polypropylene separators (25 μm , Celgard 2500) and the PY-PBI-800 electrodes as anodes inside an argon-filled glovebox (UNICO UN 650F) whose moisture and O_2 content was <0.1 ppm. Commercial LiCoO_2 electrodes with 1.5 mAhcm^{-2} of areal capacity was used as cathode for the fabrication of full cells.

3.3 Battery testing: Cyclic Voltammetry (CV) was performed in the potential range 0.01–2.1 V vs Li/Li^+ at a scan rate of 0.1 mVs^{-1} at 25 $^{\circ}\text{C}$. The scan rate dependent CV studies were carried out at 0.1, 0.3, 0.5, 0.7, and 1.0 mVs^{-1} . The electrochemical impedance spectra (EIS) were recorded in the frequency range from 1 MHz to 0.1 Hz with a sinus amplitude of 10 mV. The EIS and CV were carried out in Bio-Logic-VSP potentiostat equipped with frequency response analyzer from Bio-Logic Science Instruments Ltd.

The charge discharge studies for half-cells were performed in a galvanostatic mode using compact charge and discharge system of EC Frontier; ECAD-1000, in the potential range of 0.01–2.1 V vs Li/Li^+ at 25 $^{\circ}\text{C}$. The long cycling studies at higher current rates of 10C, 20C, 30C, 50C were performed after precycling them for 3 cycles at 0.1, 0.2, 0.5, 1, and 2C lower current rates.

The full cells were fabricated using commercial lithium cobalt oxide (LiCoO_2) as cathode with a capacity of 1.5 mAhcm^{-2} , 1.0 M LiPF_6 in EC/DEC= 50/50 (v/v) as electrolyte, polypropylene separators ($25 \mu\text{m}$, Celgard 2500), and anodes coated in the procedure exactly as mentioned for anodic half cells except the thickness of electrode was varied to 5.6 mgcm^{-2} . The full cells were cycled in the voltage range 2.4-4.2 V in CCCV mode (CCCV: Charging at Constant Current followed by charging at Constant Voltage at 4.2 V for 1 hour, then discharging at constant current).

3.4 Post cycling analysis of half-cells: The coin cell was decripped after 1500 long cycles at 2C in an argon filled glove box and the anodes (PY-PBI-800 and graphite) were washed with fresh EC: DEC with lot of care so that the SEI will not be damaged. XPS and FESEM measurements were performed on these anodes.

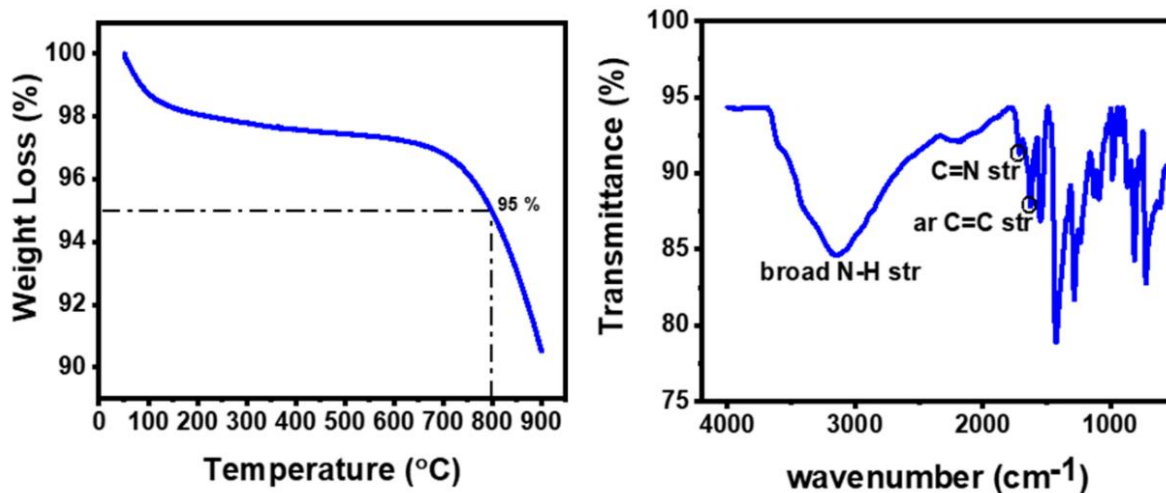


Fig. S1: Thermogravimetric Analysis (TGA) Fig. S2: FT-IR of poly-(2,5-benzimidazole) of PY-PBI-800

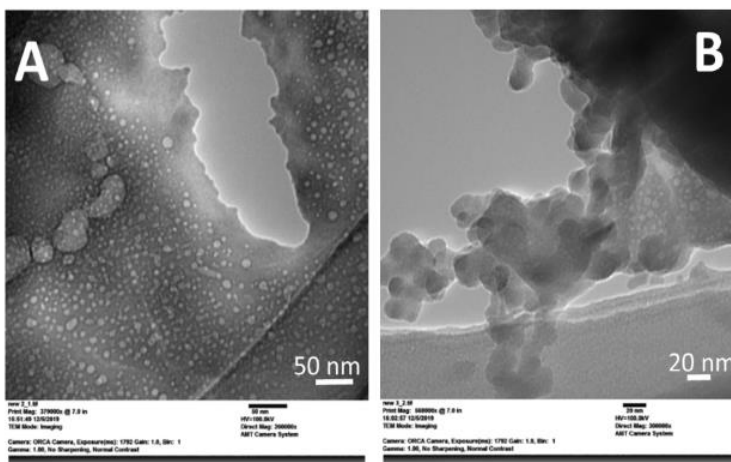


Fig. S3 TEM images of PY-PBI-800 (A) at 50 nm (B) 20 nm

Element	Area	Sensitivity factor	Atomic %	Weight %
C	24725	1	84.5	82.3
N	7077	1.63	14.9	16.9
O	395	2.33	0.6	0.8

Table S1: Elemental composition of PY-PBI-800 using XPS

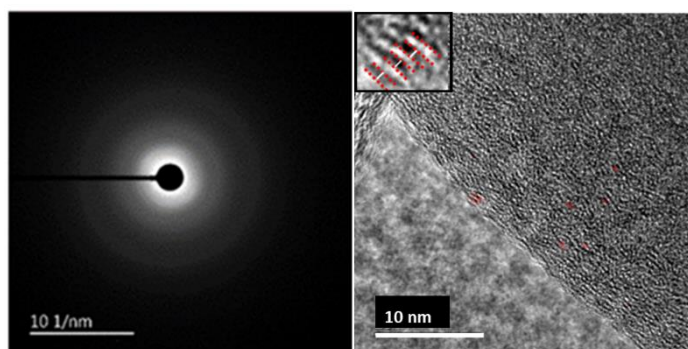


Fig. S4 (A) SAED pattern (B) HR-TEM image (for lattice spacing calculation) of PY-PBI-800

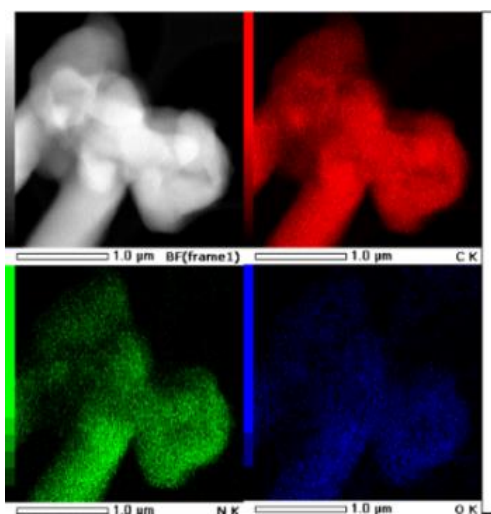


Fig. S5 STEM-EDS elemental mapping of PY-PBI-800

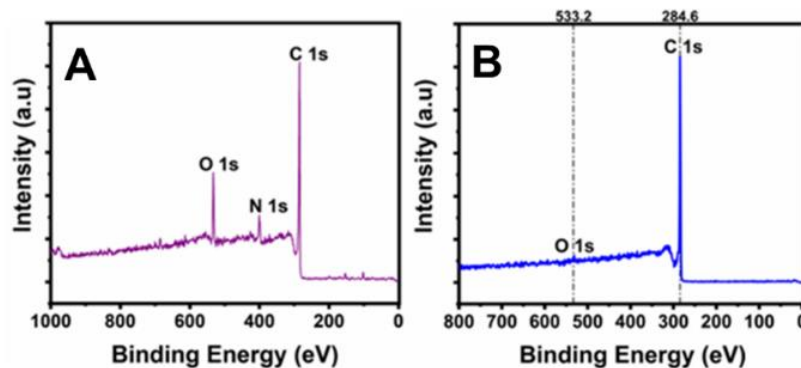


Fig. S6 XPS survey spectrum of (A) PY-PBI-800 (B) Graphite

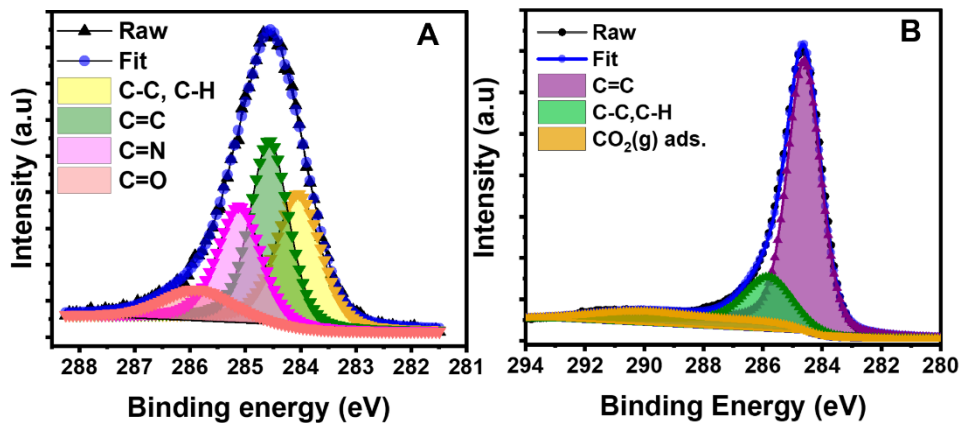


Fig. S7 Deconvoluted C1s peak of (A) PY-PBI-800 (B) Graphite

Component	Binding Energy value (eV) (PY-PBI-800)	% Area under the peak (PY-PBI-800)	Binding Energy value (Graphite)	% Area under the peak (Graphite)
C-C, C-H	284.00	30.86 %	285.8	18.24 %
C=C	284.5	35.40 %	284.6	75.46 %
C=N	285.1	24.76. %	-	-
C=O	285.9	8.98. %	290.2 (CO ₂ (g) ads.)	6.30 %

Table S2: Relative intensities of deconvoluted C1s spectra of (A) PY-PBI-800 (B) Graphite

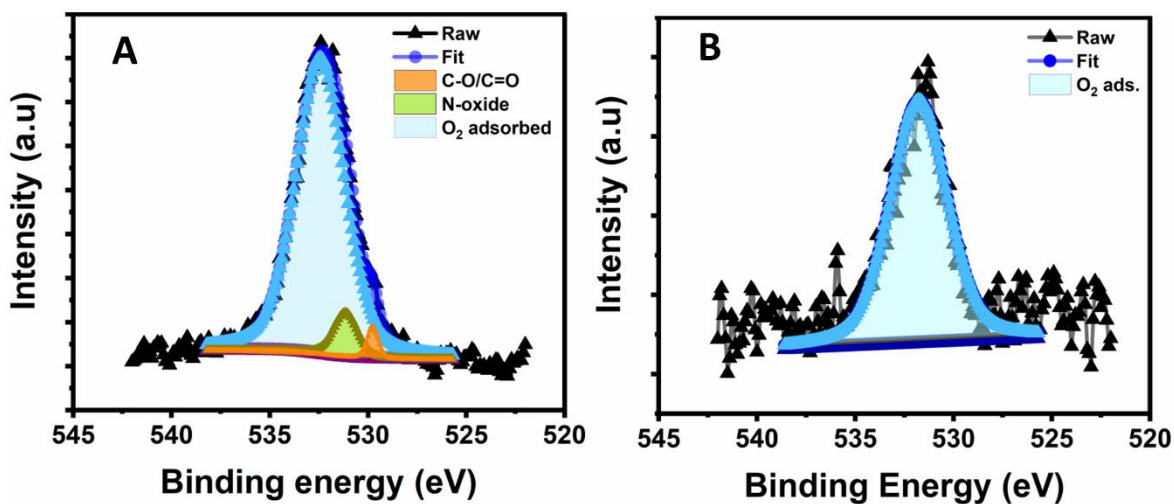


Fig. S8 Deconvoluted O1s peak of (A) PY-PBI-800 (B) Graphite

	Binding Energy value (eV) (PY-PBI-800)	% Area under the peak (PY-PBI-800)	Binding Energy value (Graphite)	% Area under the peak (Graphite)
C-O/ C=O	529.7	2.00 %	-	-
N-oxide	531.1	7.00 %	-	-
O ₂ ads.	532.4	91.00 %	531.7	100.00 %

Table S3: Relative intensities of deconvoluted O1s spectra of (A) PY-PBI-800 (B) Graphite

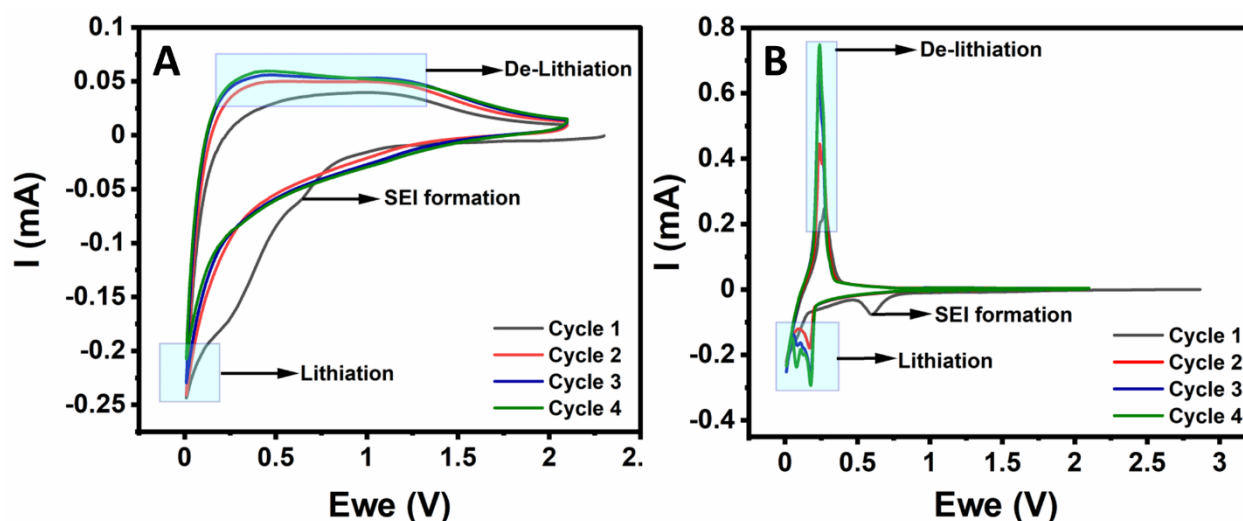


Fig. S9 Cyclic voltammogram of (A) PY-PBI-800 (B) Graphite based anodic half cells

The pre-cycling was performed at various current rates viz. 0.02, 0.04, 0.07, and 0.20 Ag⁻¹ current densities until the coulombic efficiency was >99.5 %. Fig. S10 shows the long cycling profiles after pre-cycling the anodic half cells at 0.02, 0.04, 0.07 and 0.2 Ag⁻¹ current densities respectively. It was observed that activation of the anode was faster in case of half-cell pre-cycled at a slow rate of 0.02 Ag⁻¹ wherein the cell showed peak performance within the first 50 cycles at 0.74 Ag⁻¹.

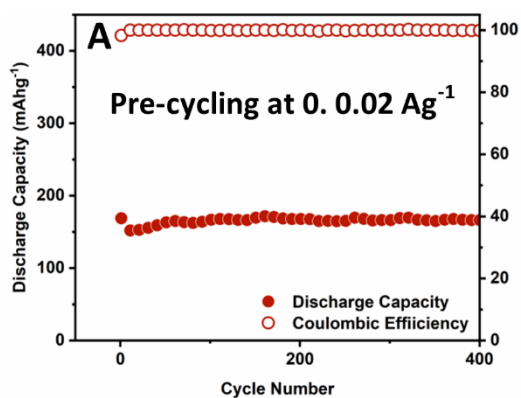


Fig. Long Cycling at 0.74 Ag^{-1} for precycling at 0.02 Ag^{-1}

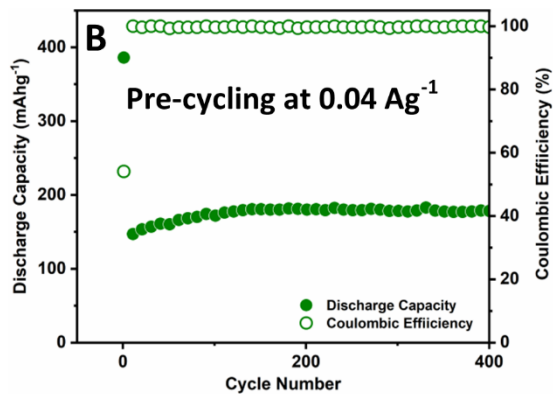


Fig. Long Cycling at 0.74 Ag^{-1} for precycling at 0.04 Ag^{-1}

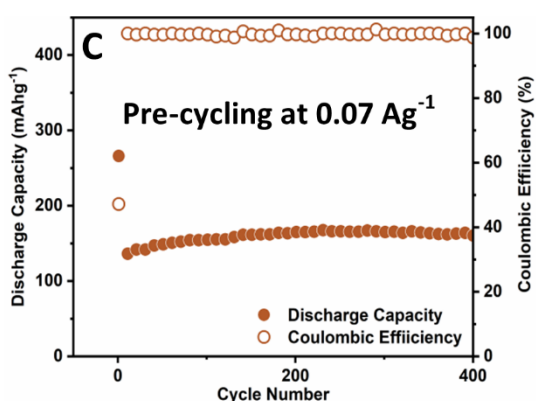


Fig. Longcycling at 0.74 Ag^{-1} for precycling at 0.074 Ag^{-1}

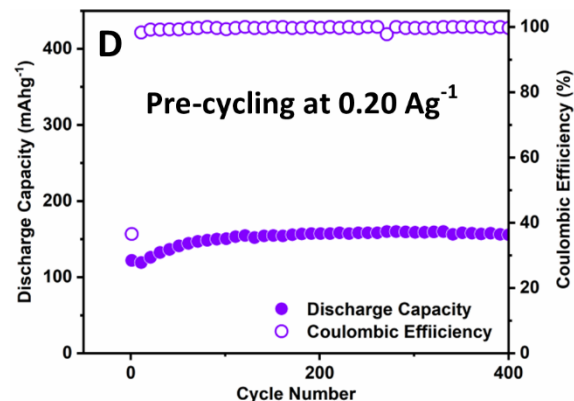


Fig. Long Cycling at 0.74 Ag^{-1} for precycling at 0.19 Ag^{-1}

Fig. S10 Long Cycling at 0.74 Ag^{-1} for pre-cycling performed at (A) 0.02 Ag^{-1} (B) 0.04 Ag^{-1} (C) 0.07 Ag^{-1} (D) 0.20 Ag^{-1} of PY-PBI-800 based anodic half cells

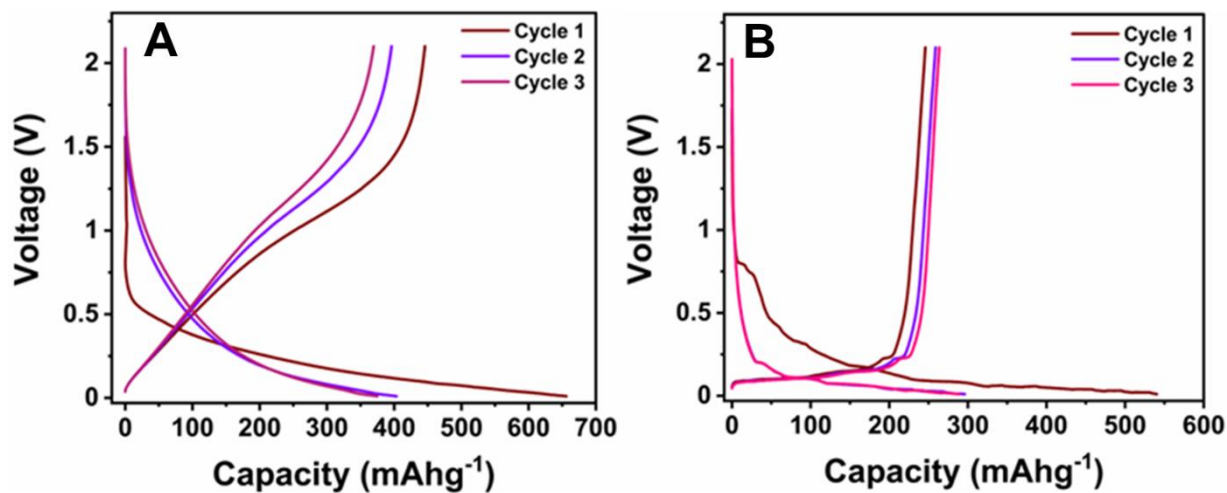


Fig. S11 Charge-Discharge curves of anodic half-cell for precycling at 0.02 Ag^{-1} (A) PY-PBI-800 (B) Graphite based anodic half cells

Sl.no	Current (A.g ⁻¹)	Capacity (mAhg ⁻¹)		Capacity Retention (%)		Time for charge and discharge (in mins)
		500 Cycles	1000 Cycles	500 Cycles	1000 Cycles	
1	0.37 A. g ⁻¹	252	230	95	87	78.2
2	0.74 A. g ⁻¹	164	153	95	89	26.1
4	3.7 A.g ⁻¹	92	86	100	90.2	3
5	7.4 A.g ⁻¹	63	55	95	98	1
6	11.1 A. g ⁻¹	53	51	100	98	0.5

Table S4 Details for long cycling of PY-PBI-800 at various current rates

Current Rate	Capacity retention (%) after 2000 th cycle	Capacity retention (%) after 3000 th cycle
3.7 A.g ⁻¹	84.7	80.0
7.4 A.g ⁻¹	91.5	82.0
11.1 A.g ⁻¹	94.0	90.0
18.6 A.g ⁻¹	87.0	84.0

Table S5 Details for long cycling of PY-PBI-800 at higher current rates

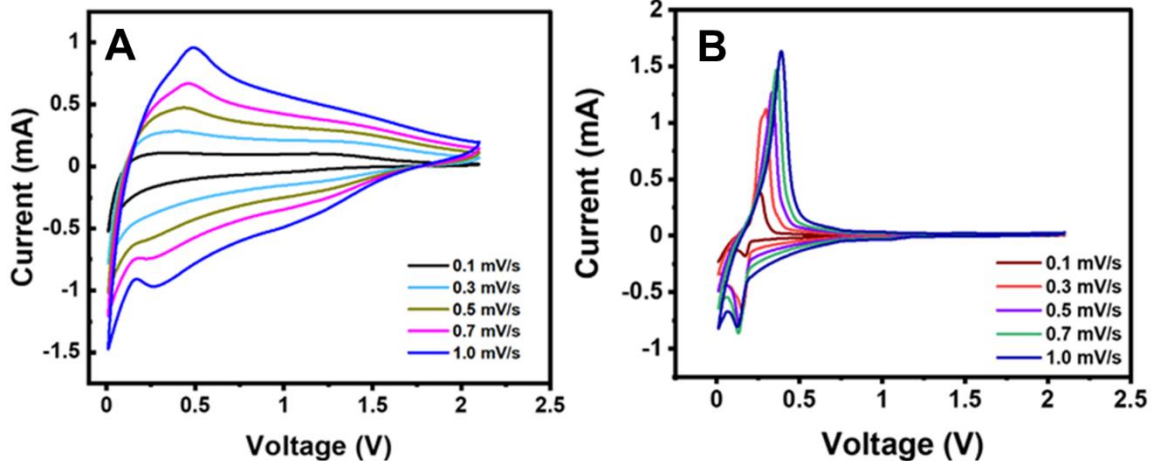


Fig. S12 Cyclic voltammetry scan rate studies of (A) PY-PBI-800 (B) Graphite anodic half cells

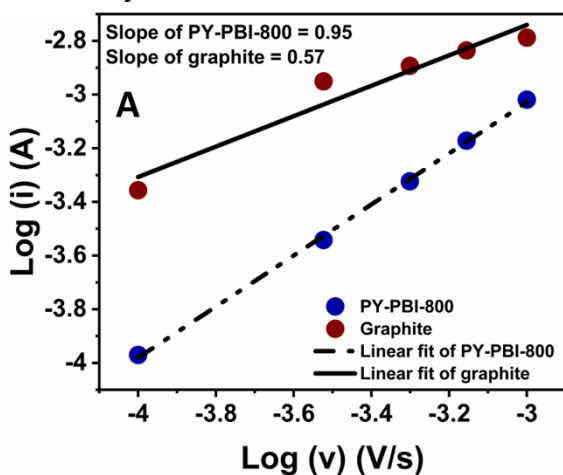


Fig. S13 Comparison of $\log(i)$ vs $\log(v)$ for PY-PBI-800 and graphite based anodic half cells

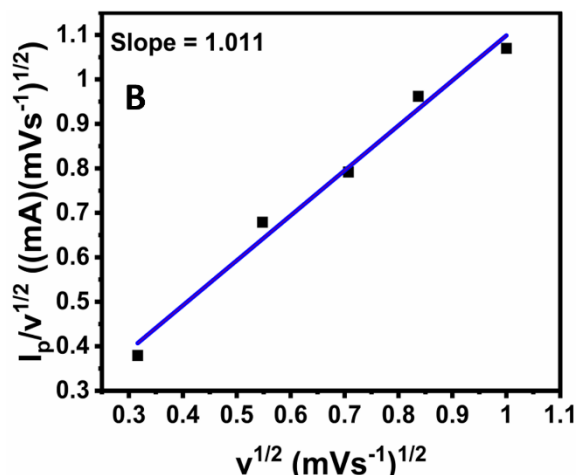


Fig. S14 Plot of $i_p/v^{1/2}$ vs $v^{1/2}$ for PY-PBI-800 based anodic half-cell

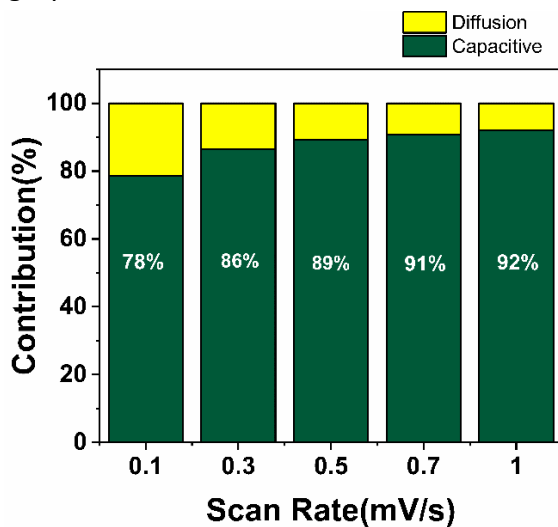


Fig. S15 Contribution of diffusion-based charge storage and pseudocapacitance-based charge storage in PY-PBI-800 based anodic half cell

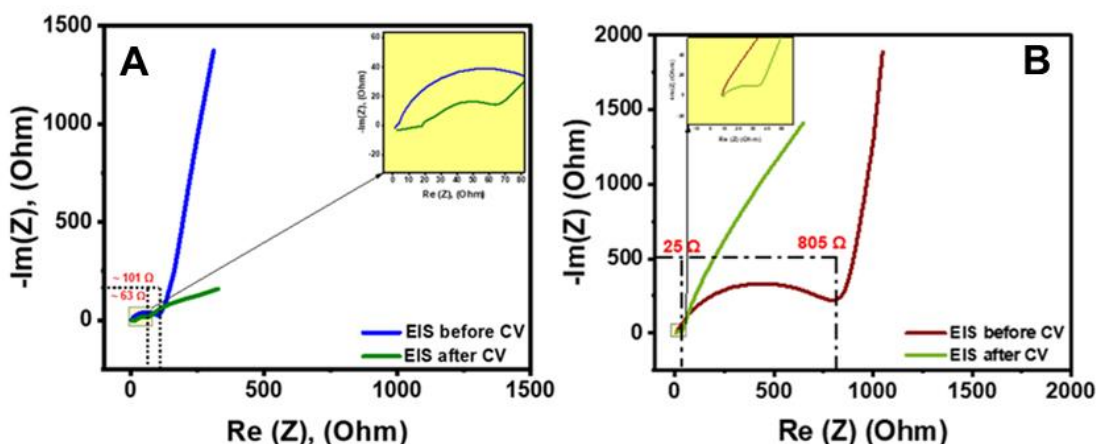


Fig. S16 Nyquist plots for (A) PY-PBI-800 (B) Graphite anodic half cells

Fig. S16 shows the Nyquist plots of the anodic half cells. The Nyquist plot consists of a semicircle related to the intersection between the high frequency semicircle and x-axis representing electrolyte resistance (R_s -high frequency range), the diameter of the depressed circle corresponds to the charge transfer resistance (R_{ct} -medium frequency region), and the straight line corresponds to the Warburg impedance of Li-ion diffusion into the bulk material (W -low frequency region). The semicircle diameter of PY-PBI-800 based anodic half-cell is larger before cycling (101 Ω) than the semicircle diameter after cycling (63 Ω) whereas in graphite before cycling, the impedance was 805 Ω which reduced to 25 Ω after cycling. The decrease in resistance after cycling can be attributed to the formation of a solid electrolyte interphase (SEI) at the electrode/electrolyte during cycling which supports in easier charge transfer and higher electrical conductivity.

Deconvolution was performed for C, N, O, and F peaks of XPS to understand the SEI composition. The deconvolution of C1s core spectra (Fig. S17A,B) indicated six conventional peaks corresponding to C-Li (intercalated Li), C=C of carbon, C-O, C=O, lithium carbonates and alkyl carbonates peaks at 284.0, 284.6, 285.3, 286.4, 288.7 and 289.9 eV which were common in both PY-PBI-800 and graphite. Corresponding peaks indicating decomposition products of electrolyte appeared in O 1s peak deconvolution (Fig. S18A,B). Decomposition of Li salt; LiPF₆ can be diagnosed by the deconvoluted F 1s core spectra (Fig. S19A,B). Two peaks at ~684.8 and ~687.2 eV corresponding to LiF, Li_xPF_y/Li_xPO_yF_z forming the inorganic portion of SEI could be identified. Table S6,7,8 show the percentage area under C 1s, F 1s, and O 1s spectra.

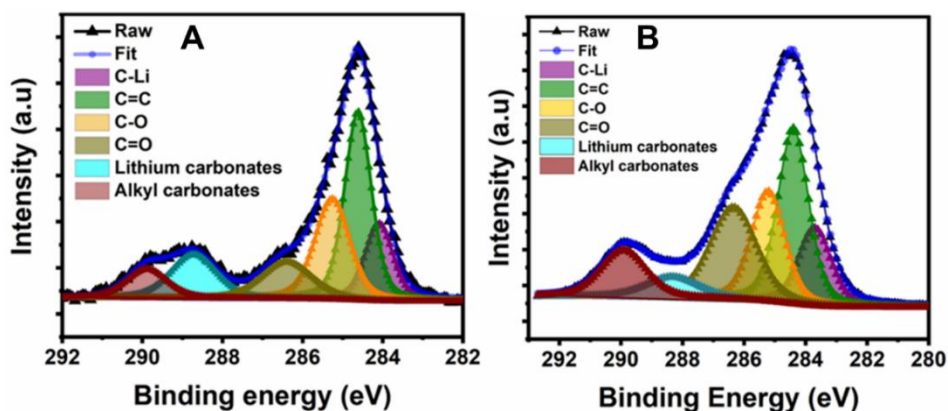


Fig S17 (A) Deconvoluted C 1s spectra of anode cycled at 0.74 Ag^{-1} for 1500 cycles (A) PY-PBI-800 (B) Graphite

Component	Binding Energy value (eV) (PY-PBI-800)	% Area under the peak (PY-PBI-800)	Binding Energy value (Graphite)	% Area under the peak (Graphite)
C-Li	284.0	13.5	283.7	13.0
C=C of active material	284.6	32.0	284.4	28.5
C-O	285.3	22.0	285.2	19.3
C=O	286.4	12.0	286.3	22.0
Lithium carbonates	288.7	13.0	288.3	5.9
Alkyl carbonates	289.9	8.0	289.9	11.0

Table. S6 Details of deconvolution of C 1s of PY-PBI-800 and graphite anode cycled at 0.74 Ag^{-1} for 1500 cycles

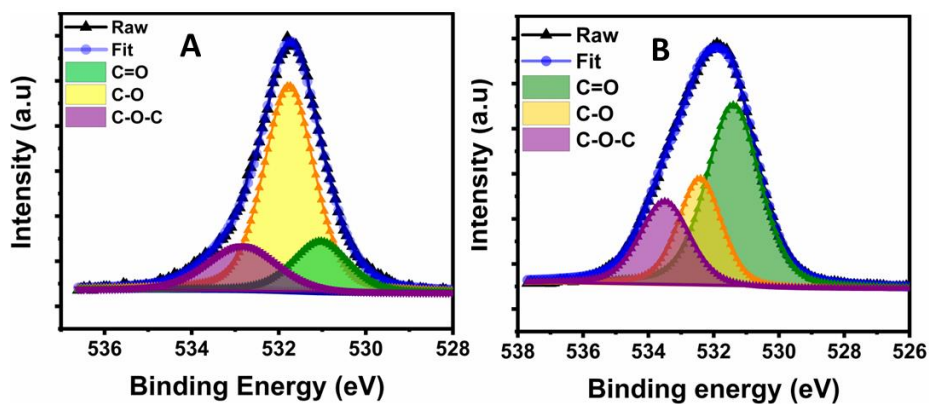


Fig. S18 Deconvoluted of O 1s spectra of anode cycled at 0.74 Ag^{-1} for 1500 cycles (A) PY-PBI-800 (B) Graphite

Component	Binding Energy value (eV) (PY-PBI-800)	% Area under the peak (PY-PBI-800)	Binding Energy value (Graphite)	% Area under the peak (Graphite)
C=O	531.0	24.6	531.4	53.0
C-O	531.7	57.3	532.4	25.0
C-O-C	532.8	18.1	533.5	22.0

Table. S7 Details of deconvolution of O1s of PY-PBI-800 and graphite anode cycled at 0.74 Ag⁻¹ for 1500 cycles

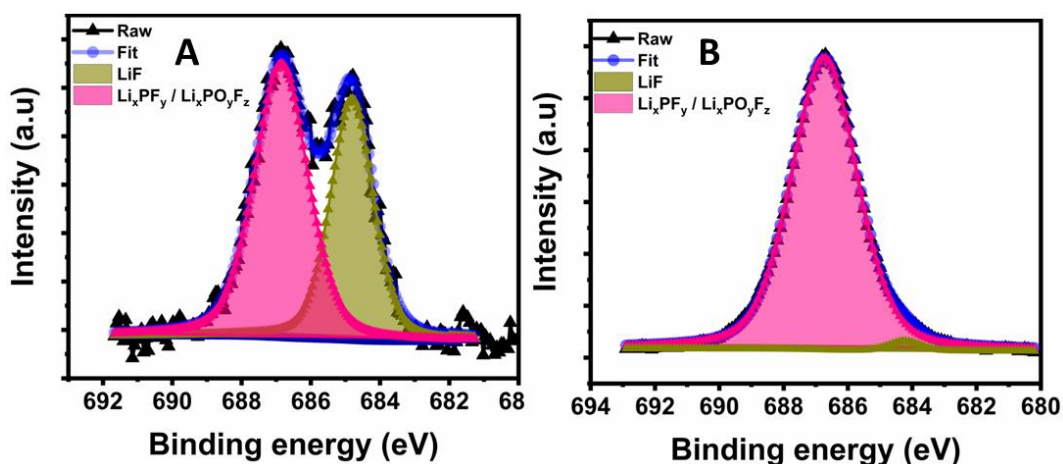


Fig. 19 Deconvolution of F1s of anode cycled at 0.74 Ag⁻¹ for 1500 cycles (A) PY-PBI-800 (B) Graphite

Component	Binding Energy value (eV) (PY-PBI-800)	% Area under the peak (PY-PBI-800)	Binding Energy value (Graphite)	% Area under the peak (Graphite)
LiF	684.8	41.0	684.2	1.3
Li _x PF _y /Li _x PO _y F _z	686.5	59.0	686.7	98.5

Table S8 Details of deconvoluted F 1s of PY-PBI-800 and graphite anode cycled at 0.74 Ag⁻¹ rate for 1500 cycles

Figure S21 shows low magnification FE-SEM micrographs of a) pristine PY-PBI-800 electrode b) PY-PBI-800 electrode cycled at 0.74 Ag^{-1} rate c) pristine graphite electrode and d) graphite electrode cycled at 0.74 Ag^{-1} rate. Fig S21 (a) indicating the pristine graphite electrode shows layered morphology, smooth surface and well-defined edges of graphite flakes. In case of cycled graphite electrode, layered morphology and well-defined flaky edges are not clearly visible due to SEI formation. Further, the surface of graphite flakes are rough with deposits of thick SEI. But in the case of cycled PY-PBI-800 electrode, as seen in Fig.S21 (c), particle shape, surface smoothness and distinct particle boundaries are retained even after 1500 cycles compared to the pristine one as shown in Fig. S21 (d). This can be ascribed to the formation of a thinner SEI layer on PY-PBI-800 electrode. The visible contrast difference in the electrode images before and after cycling is due to non-conducting SEI formation after long cycling. Also, as shown in Fig. S21 (b), absolutely no trace of cracks could be spotted on cycled PY-PBI-800 anodes indicating that the electrode retained its intact morphology without any morphological damages even after fast charge-discharge. Contrarily, micro-cracks could be traced on graphite anodes indicating the instability of the electrode while cycling at higher current rates. The undisturbed surface morphology of PY-PBI-800 based anode is another indication of its structural stability during long cycling at high rate. The cross-sections of pristine and cycled electrodes were also probed using FE-SEM. Fig. S20 shows the high magnification micrographs of pristine and cycled electrodes confirming that there are no large cracks on both the electrodes. Fig. S22 shows the cross-sectional FE-SEM images of pristine and cycled electrodes of PY-PBI-800 and graphite. Fig. S22 (a) and (b) show that the porosity in PY-PBI-800 electrode was almost retained even after long cycling. Whereas Fig. S22 (c) and (d) clearly indicate the loss in porosity of graphite electrode after long cycling.

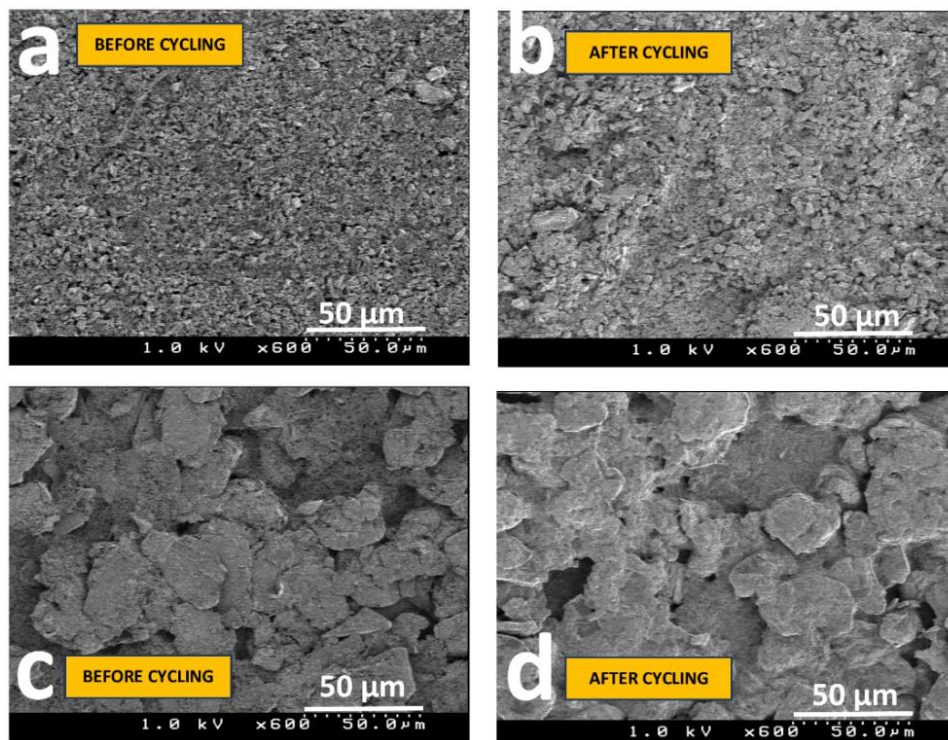


Fig.S20 Comparison of the FE-SEM images at 50 μm of electrodes before cycling and after cycling at 0.74 Ag^{-1} for ~ 1500 cycles (a, b) PY-PBI-800 (c, d) graphite

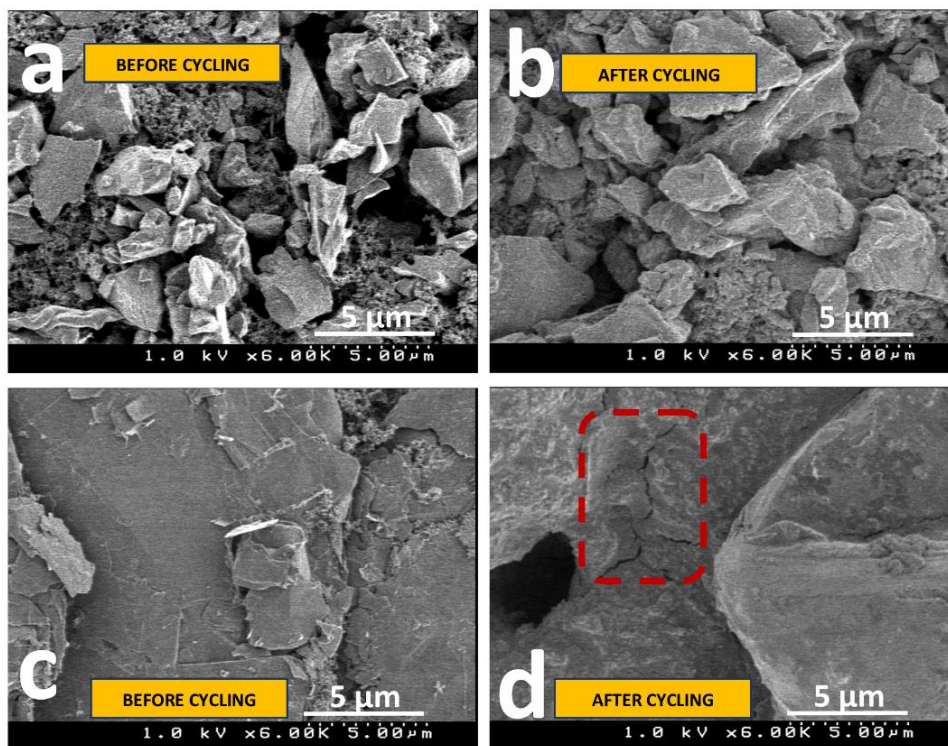


Fig. S21 Comparison of the FE-SEM images at 5 μm of electrodes before cycling and after cycling at 0.74 Ag^{-1} for ~ 1500 (a, b) PY-PBI-800 (c, d) graphite

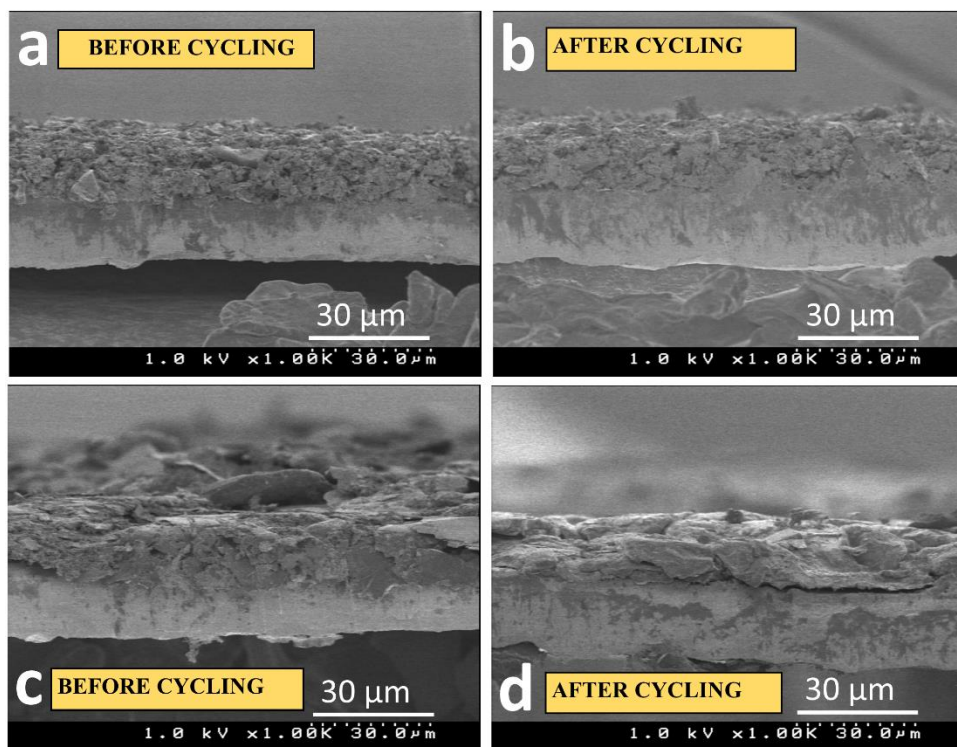


Fig. S22 Comparison of the FE-SEM images at 30 μm of electrodes before cycling and after cycling at 0.74 Ag^{-1} for ~ 1500 (a, b) PY-PBI-800 (c, d) graphite

Cycling numbers	Discharge capacity (mAh)	Capacity retention
1st	1.69	-
10th	1.65	97.6%
50th	1.55	91.7%
100th	1.49	88.1%
150th	1.46	86.4%
200th	1.44	85.2%
300th	1.39	82.2%
350th	1.35	79.9%
400th	1.30	76.9%

Table S9 Specific values of capacity and capacity retention for PY-PBI-800/ LiCoO_2 based full cells

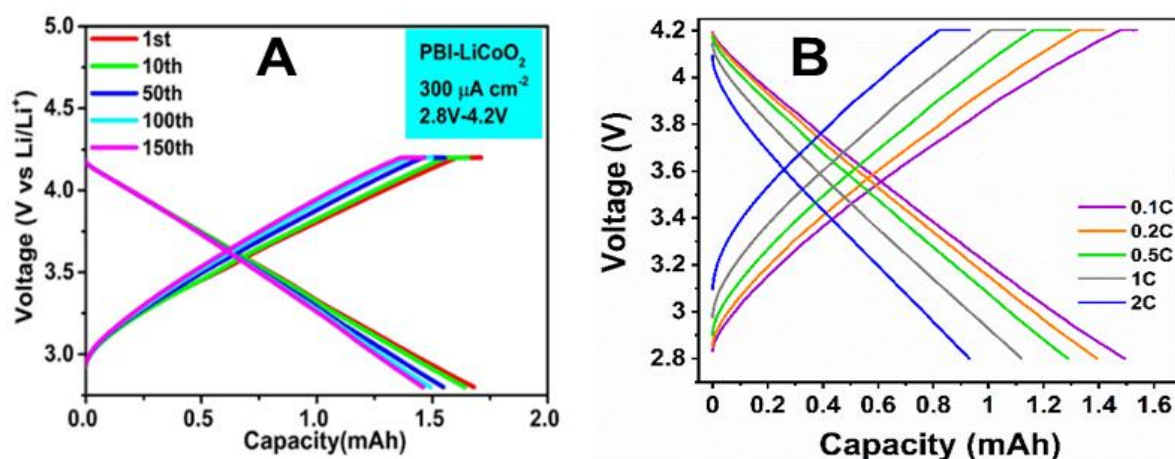


Fig. S23 Charge-Discharge curves of PY-PBI-800 based full cell (A) long cycling at $300\mu\text{Acm}^{-2}$ (B) rate studies

REAGENT NAME	SOURCE	PRICE	REQUIRED AMOUNT	PRICE FOR REQUIRED AMOUNT (in \$)
3,4 DIAMINOBENZOIC ACID (3,4 DABA)	SIGMA	1.647 \$/g	110.5 g	182.04
METHANOL	WAKO	0.010 \$/mL	973 mL	10.29
CONC. HCL	WAKO	0.015 \$/mL	50 mL	0.75
POLYPHOSPHORIC ACID	SIGMA	0.085 \$/g	2865 g	242.31
POTASSIUM HYDROXIDE	WAKO	0.023 \$/g	955 g	21.87
			Total	457.30 \$

Table S10 Details on cost estimation for synthesis of 100g of PY-PBI-800

The cost in terms of lab scale preparation of 100g of PY-PBI-800 carbon material was calculated (Table S10) and was found to be $\sim 4.57 \text{ \$g}^{-1}$ based on chemicals purchased for regular usage at lab. Since AB-PBI can be synthesized using bio-derivable monomer 3,4 DABA, the overall cost for synthesis can be even cheaper. However, the authors also believe that, at industrial scale the price accounted for synthesis of 100 g of carbon could be much cheaper. We also noticed that preparation of PY-PBI-800 costs much cheaper than the commercially available N-doped graphene powder which costs $225 \text{ \$g}^{-1}$ (Advanced Chemical Supplier, US. CAS No.: 7782-42-5). This shows the cost of PY-PBI-800 is almost 50 times lower than that of its counterpart i.e., nitrogen doped graphene.

- All the costs of chemicals have been converted into \$/g or \$/mL from the local cost (¥/g or ¥/mL).

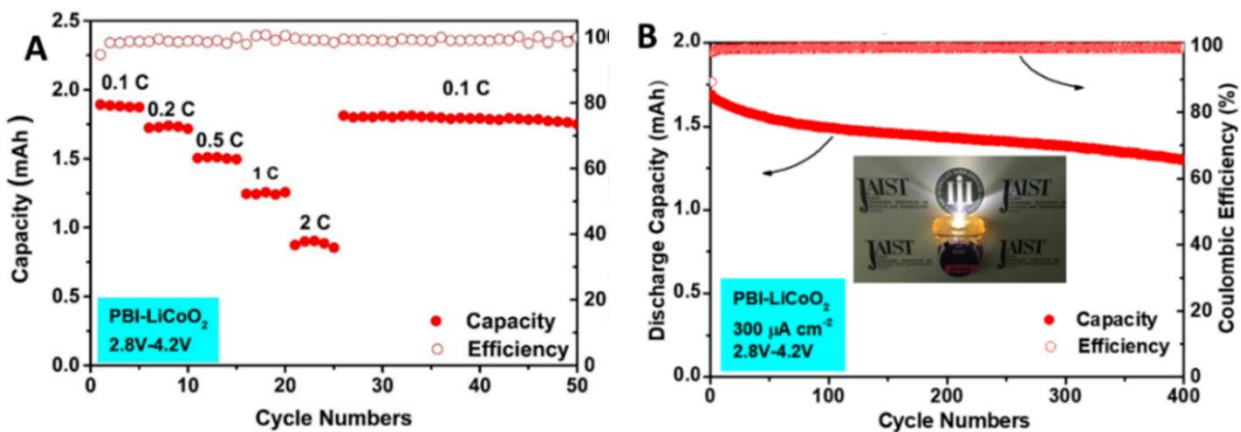


Fig. S24: PY-PBI-800/LiCoO₂ based full cells (A) Rate studies at different current rates (B) Long cycling ability at 0.2C for 400 cycles (inset: Demonstration of LED light lit using PY-PBI-800/LiCoO₂ based full cell)

References:

- 1 R. Nandan, A. Gautam and K. K. Nanda, *J. Mater. Chem. A*, 2018, **6**, 20411–20420.